Inversion formulas for the broken-ray Radon transform

2011 Inverse Problems 27 025002

(http://iopscience.iop.org/0266-5611/27/2/025002)

Inverse Problems **27** (2011) 025002 (13pp) doi:10.1088/0266-5611/27/2/025002

Inversion formulas for the broken-ray Radon transform

Lucia Florescu[1], **Vadim A Markel**[2] **and John C Schotland**[3]

[1] Department of Bioengineering, University of Pennsylvania, Philadelphia, PA 19104, USA
[2] Department of Radiology and Graduate Group in Applied Mathematics and Computational Science, University of Pennsylvania, Philadelphia, PA 19104, USA
[3] Department of Mathematics, University of Michigan, Ann Arbor, MI 48109, USA

E-mail: schotland@umich.edu

Received 24 August 2010, in final form 24 November 2010
Published 6 January 2011
Online at stacks.iop.org/IP/27/025002

Abstract
We consider the inversion of the broken-ray Radon transform, a problem that arises in the context of inverse transport theory in optical tomography. We derive inversion formulas which allow the recovery of the scattering and absorption coefficients of the radiative transport equation in the single-scattering regime. Our results are illustrated with numerical simulations.

(Some figures in this article are in colour only in the electronic version)

1. Introduction

The inverse transport problem consists of recovering the spatially varying absorption and scattering coefficients of the interior of a highly scattering medium from measurements taken on its boundary [2]. The problem has been widely studied in the context of optical tomography (OT)—a biomedical imaging modality that makes use of multiply-scattered light to visualize structural variations in the optical properties of tissue[1]. OT provides unique capabilities to assess the physiological function including blood volume and tissue oxygenation.

The propagation of light in a random medium, taken to be the domain $\Omega \subset \mathbb{R}^3$, is governed by the radiative transport equation (RTE):

$$\hat{\mathbf{s}} \cdot \nabla I + (\mu_a(\mathbf{r}) + \mu_s(\mathbf{r}))I = \mu_s(\mathbf{r}) \int p(\hat{\mathbf{s}}, \hat{\mathbf{s}}')I(\mathbf{r}, \hat{\mathbf{s}}')\, \mathrm{d}^2 s', \qquad \mathbf{r} \in \Omega. \tag{1}$$

Here $I(\mathbf{r}, \hat{\mathbf{s}})$ denotes the specific intensity at the point $\mathbf{r} \in \Omega$ in the direction $\hat{\mathbf{s}}$, and μ_a and μ_s are the absorption and scattering coefficients of the medium. The phase function p is symmetric under the interchange of its arguments and normalized so that $\int p(\hat{\mathbf{s}}, \hat{\mathbf{s}}')\, \mathrm{d}^2 s' = 1$ for all $\hat{\mathbf{s}}$. The specific intensity is also assumed to obey the half-range boundary condition

$$I(\mathbf{r}, \hat{\mathbf{s}}) = I_{\mathrm{inc}}(\mathbf{r}, \hat{\mathbf{s}}), \qquad (\mathbf{r}, \hat{\mathbf{s}}) \in \Gamma_-(\Omega), \tag{2}$$

where I_{inc} is the incident-specific intensity. We have introduced the sets $\Gamma_\pm(\Omega) = \{(\mathbf{r}, \hat{\mathbf{s}}) : \pm\mathbf{r} \cdot \hat{\mathbf{n}} > 0\}$, where $\hat{\mathbf{n}}$ is the outward unit normal to $\partial\Omega$.

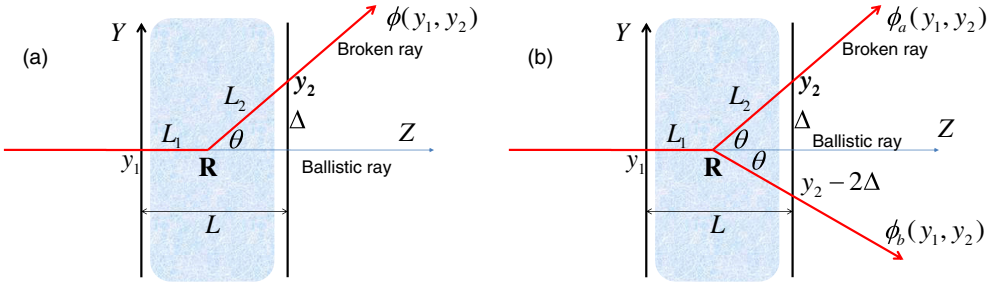

Figure 1. Illustrating the geometry of a broken ray.

The inverse problem of optical tomography is to recover the pair of coefficients (μ_a, μ_s) from outgoing measurements of the specific intensity on $\Gamma_+(\Omega)$. Here we assume that the phase function is known and has no spatial dependence. We introduce the albedo operator $\mathcal{A} : I_{\text{inc}} \mapsto I|_{\Gamma_+}$. If $\mathcal{A}$ is known, then (μ_a, μ_s) can be reconstructed uniquely [4, 5, 9, 10]. This result follows from analyzing the singularities of the albedo operator. The singular structure can be used to recover (μ_a, μ_s) with the Holder stability. It is important to note that angularly resolved measurements of the specific intensity are difficult to obtain in practice. The inverse problem with angularly averaged data or partial angular data can be seen to be severely ill-posed [2]. The effect of angular averaging is to destroy the singularities that are present in the albedo operator. At best, it is possible to reconstruct the low-frequency parts of (μ_a, μ_s) with logarithmic stability [2].

The albedo operator can be decomposed into a sum whose terms correspond to successively higher orders of scattering. The lowest order term, which accounts for the propagation of unscattered photons, is the most singular. The next term, which corresponds to single-scattered photons (whose paths are the broken rays illustrated in figure 1) is less singular. The higher-order terms are increasingly smooth at each order of scattering.

In [6, 7] we considered the problem of imaging an optically thin medium in the single-scattering regime. In this method, which we refer to as single-scattering optical tomography (SSOT), the specific intensity is related to the integral of the attenuation coefficient $\mu_t = \mu_a + \mu_s$ along a broken ray. The aforementioned integral defines the broken-ray Radon transform of μ_t, which is parametrized by the positions and directions of the source and detector in an SSOT experiment.

We have studied the problem of recovering (μ_a, μ_s) by numerical inversion of the broken-ray Radon transform [6]. By making use of singular-value analysis, it was found that this inverse problem is mildly ill-posed, even if only two directions of measurement are employed. In this work, we further explore this counterintuitive result by deriving explicit inversion formulas for the broken-ray Radon transform and further investigating its mathematical structure. The inversion formulas are tested in numerical simulations which illustrate the nature of the singularities of the inverse problem.

The remainder of this paper is organized as follows. In section 2, the broken-ray transform is defined and some relevant geometrical quantities are introduced. In section 3, inversion formulas are derived for two cases: (i) assuming the medium has a spatially varying absorption coefficient and a constant scattering coefficient (section 3.1) and (ii) assuming the medium has spatially varying absorption and scattering coefficients (section 3.2). Numerical simulations are presented in section 4. Finally, section 5 contains a discussion and a brief summary of our results.

2. The broken-ray Radon transform

The physics of the broken-ray Radon transform was discussed in [6]. The geometry of a broken ray is illustrated in figure 1 for the case of a normally incident beam in the slab geometry. Here we focus on the inverse problem of SSOT. We note that image reconstruction in SSOT is performed slice-by-slice. A slice is determined by the direction vectors of the sources and detectors, which are assumed to lie in the same plane. In the reference frame of figure 1, the slices correspond to the planes $x = \text{const}$. Note that once a slice is selected, the source and detector direction vectors are fixed. However, the positions of the sources and detectors can be varied along the y-axis, subject to the constraint that the vertex $\mathbf{R}$ (the ray turning point) lies within the slab $0 \leqslant z \leqslant L$. The position of the source is denoted by y_1 and the position of the detector by y_2; every distinct source–detector pair (y_1, y_2) corresponds to a unique broken ray. The integral of the attenuation coefficient along a broken ray defines the data function $\phi(y_1, y_2)$ which is given by

$$\int_{\mathrm{BR}(y_1,y_2)} \mu_t(\mathbf{r}(\ell))\,\mathrm{d}\ell - \ln\frac{\mu_s(\mathbf{R}(y_1, y_2))}{\bar{\mu}_s} = \phi(y_1, y_2), \tag{3}$$

as described in [6]. Here $\bar{\mu}_s$ is the background scattering coefficient of the medium, the integral is evaluated along the broken ray $\mathrm{BR}(y_1, y_2)$, $\mathbf{r}$ is a two-dimensional position vector in the yz-plane, and $\mathbf{R}(y_1, y_2)$ is the ray turning point. The inverse problem of SSOT is to recover μ_t and μ_s from $\phi(y_2, y_1)$. The absorption coefficient μ_a can then be determined from the difference between μ_t and μ_s. We note that if $\mu_s = \bar{\mu}_s$, then (3) becomes

$$\int_{\mathrm{BR}(y_1,y_2)} \mu_t(\mathbf{r}(\ell))\,\mathrm{d}\ell = \phi(y_1, y_2), \tag{4}$$

which defines the broken-ray Radon transform of μ_t.

Suppose that the scattering coefficient is constant and the absorption coefficient is spatially varying. Then we will see that it is sufficient to consider a family of broken rays in which $y_2 > y_1$. We denote the transverse source–detector separation by $\Delta = y_2 - y_1$. If the angle between the illumination and detection directions is θ, then Δ varies in the interval $(0, \Delta_{\max})$, where $\Delta_{\max} = L\tan\theta$. The broken ray shown in figure 1(a) consists of two segments of length L_1 and L_2, respectively, where

$$L_1(\Delta) = L - \Delta\cot\theta = L(1 - \Delta/\Delta_{\max}), \tag{5a}$$

$$L_2(\Delta) = \Delta\csc\theta = (\Delta/\Delta_{\max})\sqrt{L^2 + \Delta_{\max}^2}. \tag{5b}$$

Next, suppose that the absorption and the scattering coefficients are both spatially varying. In this case, measurements of the type shown in figure 1(a) are insufficient to reconstruct both coefficients simultaneously. However, if two broken rays with a common vertex, as shown in figure 1(b) are used, the inverse problem is formally determined and we will see that the pair (μ_a, μ_s) can be uniquely recovered.

The measurement scheme described above is suitable for reconstructing an image in the rectangular area defined by the inequalities $0 \leqslant z \leqslant L$ and $y_{\min} \leqslant y \leqslant y_{\max}$, where L is the depth of the slab, and $y_{\min}$, $y_{\max}$ are determined by the window in which the sources and detectors are scanned.

3. Inversion formulas

3.1. Spatially uniform scattering

If the scattering coefficient is spatially uniform, $\mu_s = \bar{\mu}_s$, then the logarithmic term on the left-hand side of equation (3) vanishes. The image reconstruction problem is thus reduced to recovering the function $\mu_t(y, z)$ from the integral equation

$$\int_{\mathrm{BR}(y_1,y_2)} \mu_t[y(\ell), z(\ell)]\,\mathrm{d}\ell = \phi(y_1, y_2). \tag{6}$$

It is convenient to introduce the change of variables

$$y_1 = w, \qquad y_2 = w + \Delta, \tag{7}$$

and define a new data function according to

$$\psi(w, \Delta) \equiv \phi(w, w + \Delta). \tag{8}$$

Thus, we parametrize the data by the position of the source, w, and by the transverse source–detector separation, Δ. Therefore, we can write

$$y(\ell) = w + \eta(\Delta, \ell), \qquad z(\ell) = \zeta(\Delta, \ell), \tag{9}$$

where the functions $\eta(\Delta, \ell)$, $\zeta(\Delta, \ell)$ are independent of w. Taking the Fourier transform of (6) with respect to w, we obtain the analog of the Fourier-slice theorem:

$$\int_0^{L_1(\Delta)+L_2(\Delta)} \mathrm{e}^{-\mathrm{i}k\eta(\Delta,\ell)}\tilde{\mu}_t(k, \zeta(\Delta, \ell))\,\mathrm{d}\ell = \tilde{\psi}(k, \Delta), \tag{10}$$

where the Fourier transforms are defined as

$$\tilde{\psi}(k, \Delta) = \int_{-\infty}^{\infty} \psi(w, \Delta)\,\mathrm{e}^{\mathrm{i}kw}\,\mathrm{d}w, \qquad \tilde{\mu}_t(k, z) = \int_{-\infty}^{\infty} \mu_t(y, z)\,\mathrm{e}^{\mathrm{i}ky}\,\mathrm{d}y. \tag{11}$$

Thus, the two-dimensional integral equation (6) has been reduced to the one-dimensional integral equation (10), which is parametrized by the Fourier variable k.

The integral equation (10) can be solved analytically. To this end, we must specify the functions $\eta(\Delta, \ell)$ and $\zeta(\Delta, \ell)$. For the specific geometry of the broken rays shown in figure 1(a), we have

$$\eta(\Delta, \ell) = \begin{cases} 0, & \ell < L_1(\Delta) \\ [\ell - L_1(\Delta)]\sin\theta, & L_1(\Delta) < \ell < L_1(\Delta) + L_2(\Delta) \end{cases}, \tag{12a}$$

$$\zeta(\Delta, \ell) = \begin{cases} \ell, & \ell < L_1(\Delta) \\ L_1(\Delta) + [\ell - L_1(\Delta)]\cos\theta, & L_1(\Delta) < \ell < L_1(\Delta) + L_2(\Delta) \end{cases}. \tag{12b}$$

Upon substitution of these expressions into (10), we obtain

$$\int_0^{L_1(\Delta)} \tilde{\mu}_t(k, \ell)\,\mathrm{d}\ell + \frac{\mathrm{e}^{\mathrm{i}kL_1(\Delta)\tan\theta}}{\cos\theta} \int_{L_1(\Delta)}^{L} \tilde{\mu}_t(k, \ell)\,\mathrm{e}^{-\mathrm{i}k\ell\tan\theta}\,\mathrm{d}\ell = \tilde{\psi}(k, \Delta). \tag{13}$$

We can now use the degree of freedom associated with the variable Δ to invert (13) for any fixed value of k. To simplify the calculations, we introduce the notation

$$q \equiv k\tan\theta, \tag{14a}$$

$$\lambda \equiv \cot(\theta/2), \qquad c \equiv \cos\theta, \qquad \kappa = \frac{c}{1-c} = \cot(\theta/2)\cot\theta, \tag{14b}$$

$$f(z) \equiv \tilde{\mu}(q\cot\theta, z), \qquad F(z) \equiv \tilde{\psi}(q\cot\theta, (L - z)\tan\theta). \tag{14c}$$

The dependence of $f(z)$ and $F(z)$ on q is implied. Equation (13) thus takes the form

$$\int_0^z f(\ell)\,\mathrm{d}\ell + \frac{1}{c}\,\mathrm{e}^{\mathrm{i}qz}\int_z^L \mathrm{e}^{-\mathrm{i}q\ell} f(\ell)\,\mathrm{d}\ell = F(z), \qquad 0 \leqslant z \leqslant L. \tag{15}$$

In this equation, $F(z)$ is known and $f(z)$ must be found. To solve (15) for a fixed value of q, we differentiate once with respect to z and obtain the following result:

$$-\frac{1}{\kappa} f(z) + \frac{\mathrm{i}q}{c}\,\mathrm{e}^{\mathrm{i}qz}\int_z^L \mathrm{e}^{-\mathrm{i}q\ell} f(\ell)\,\mathrm{d}\ell = F'(z), \tag{16}$$

where the prime denotes differentiation. We then use (15) and (16) to construct the linear combination $G(z) = F'(z) - \mathrm{i}qF(z)$ in terms of $f(z)$. We thus have

$$-\frac{1}{\kappa} f(z) - \mathrm{i}q\int_0^z f(\ell)\,\mathrm{d}\ell = G(z). \tag{17}$$

Differentiating one more time with respect to z, we obtain the ordinary differential equation

$$f'(z) + \mathrm{i}\kappa q f(z) = -\kappa G'(z), \tag{18}$$

which has the solution

$$f(z) = \mathrm{e}^{-\mathrm{i}\kappa qz}\left[f(0) - \kappa\int_0^z \mathrm{e}^{\mathrm{i}\kappa q\ell} G'(\ell)\,\mathrm{d}\ell\right]. \tag{19}$$

We then set $z = 0$ in (17) and find that $f(0) = -\kappa G(0)$. Substituting this result into (19) and integrating once by parts, we arrive at the solution to equation (15):

$$f(z) = -\kappa\left[G(z) - \mathrm{i}\kappa q\,\mathrm{e}^{-\mathrm{i}\kappa qz}\int_0^z \mathrm{e}^{\mathrm{i}\kappa q\ell} G(\ell)\,\mathrm{d}\ell\right]. \tag{20}$$

An important remark on the above result is necessary. The function $F(z)$ in (15) is not arbitrary, but obeys the condition

$$F(L) = \mathrm{e}^{-\mathrm{i}\kappa qL}\left[cF(0) + \mathrm{i}\kappa q\int_0^L \mathrm{e}^{\mathrm{i}\kappa q\ell} F(\ell)\,\mathrm{d}\ell\right], \tag{21}$$

which can be verified by direct calculation. However, measurements from experiments in which the single-scattering approximation does not hold may result in a function $F(z)$ that does not satisfy this condition. On the other hand, (20) is invariant under addition to $F(z)$ of a function of the form $a\exp(\mathrm{i}qz)$, where a is an arbitrary constant. It can be easily seen that any function $F(z)$ can be uniquely written in the form $F(z) = F_{\mathrm{reg}}(z) + a\exp(\mathrm{i}qz)$, where $F_{\mathrm{reg}}(z)$ satisfies condition (21). Thus, the inversion formula (20) implicitly involves regularization of the data.

Restoring the original notation, we find that the solution to (13) is given by

$$\tilde{\mu}_t(k, z) = \lambda\left[H(k, z) - \mathrm{i}k\lambda\,\mathrm{e}^{-\mathrm{i}k\lambda z}\int_0^z \mathrm{e}^{\mathrm{i}\lambda k\ell} H(k, \ell)\,\mathrm{d}\ell\right], \tag{22}$$

where

$$H(k, z) \equiv \left(\frac{\partial}{\partial\Delta} + \mathrm{i}k\right)\tilde{\psi}(k, \Delta)\Big|_{\Delta=(L-z)\tan\theta}. \tag{23}$$

Next, we apply the inverse Fourier transform and obtain

$$\mu_t(y, z) = \int_{-\infty}^{\infty} \tilde{\mu}_t(k, z)\,\mathrm{e}^{-\mathrm{i}ky}\frac{\mathrm{d}k}{2\pi}, \tag{24}$$

which yields

$$\mu_t(y,z) = \lambda \left\{ \left[\frac{\partial}{\partial \Delta} - (1+\kappa)\frac{\partial}{\partial y} \right] \psi(y,\Delta) + \kappa \frac{\partial}{\partial y}\psi(y+\lambda z, \Delta_{\max}) \right. \\ \left. - \kappa(1+\kappa)\frac{\partial^2}{\partial y^2}\int_{\Delta}^{\Delta_{\max}} \psi(y+\kappa(\ell-\Delta),\ell)\,\mathrm{d}\ell \right\}\Bigg|_{\Delta=(L-z)\tan\theta}. \tag{25}$$

The above result is the required inversion formula for the broken-ray Radon transform. We note that it is the analog of the filtered backprojection formula for the inverse of the two-dimensional Radon transform.

3.2. Spatially nonuniform scattering

Simultaneous reconstruction of the scattering and absorption coefficients can be performed without making use of the entire space of positions and directions which is available in SSOT. It is sufficient, for example, to use normally incident sources and two different angles of detection for each source. A special case of this measurement scheme is illustrated in figure 1(b), where the two broken rays are assumed to have a common vertex at the point **R** and are denoted by BR_a and BR_b. The corresponding data functions are denoted by $\phi_a(y_1, y_2)$ and $\phi_b(y_1, y_2)$.

We begin the derivation of the inversion formula by eliminating the logarithmic term in (3), which is done by taking a differential measurement. The differential data function is defined as

$$\phi_d(y_1, y_2) = \phi_a(y_1, y_2) - \phi_b(y_1, y_2). \tag{26}$$

It is easy to see that $\phi_d(y_1, y_2)$ can be used to reconstruct $\mu_t(y, z)$ even when the scattering coefficient of the medium is spatially nonuniform. Indeed, because the a- and b-broken rays have the same vertex, we have

$$\int_{\mathrm{BR}_a(y_1,y_2)} \mu_t(y(\ell), z(\ell))\,\mathrm{d}\ell - \int_{\mathrm{BR}_b(y_1,y_2)} \mu_t(y(\ell), z(\ell))\,\mathrm{d}\ell = \phi_d(y_1, y_2). \tag{27}$$

The inversion of (27) can be carried out by employing the Fourier transform. We make the change of variables (7) and define the new data function as $\psi_d(w, \Delta) \equiv \phi_d(w, w + \Delta)$. The Fourier slice theorem then takes the form

$$-2\mathrm{i}\int_{L_1(\Delta)}^{L_1(\Delta)+L_2(\Delta)} \sin\left(k\eta(\Delta,\ell)\right)\tilde{\mu}_t(k, \zeta(\Delta,\ell))\,\mathrm{d}\ell = \tilde{\psi}_d(k,\Delta), \tag{28}$$

where $\eta(\Delta, \ell)$ and $\zeta(\Delta, \ell)$ are given by (12). Using these expressions and making an appropriate change of the integration variable, (28) can be rewritten as

$$-\frac{2\mathrm{i}}{\cos\theta}\int_{L_1(\Delta)}^{L} \sin\left(k(\ell - L_1(\Delta))\tan\theta\right)\tilde{\mu}_t(k,\ell)\,\mathrm{d}\ell = \tilde{\psi}_d(k,\Delta). \tag{29}$$

To solve for $\tilde{\mu}_t(k, z)$, we use the change of variables $z = L_1(\Delta)$ (equivalently, $\Delta = (L - z)\tan\theta$) and differentiate twice with respect to z. This yields

$$\tilde{\mu}_t(k,z) = \frac{\sin\theta}{2}\left(-\frac{1}{\mathrm{i}k}\frac{\partial^2}{\partial\Delta^2} + \mathrm{i}k\right)\tilde{\psi}_d(k,\Delta)\Big|_{\Delta=(L-z)\tan\theta}. \tag{30}$$

The function $\mu_t(y, z)$ is then obtained by inverse Fourier transformation. The final result is

$$\mu_t(y,z) = \frac{\sin\theta}{4}\left[\frac{\partial^2}{\partial\Delta^2}\int_{-\infty}^{\infty} \mathrm{sgn}(y-w)\psi_d(w,\Delta)\,\mathrm{d}w - 2\frac{\partial}{\partial y}\psi_d(y,\Delta)\right]\Bigg|_{\Delta=(L-z)\tan\theta}. \tag{31}$$

In the above equation, $\mathrm{sgn}(x)$ denotes the sign of x and it is assumed that the data function $\psi_d(w, \Delta)$ vanishes for $|w| > w_{\max} > 0$, so that the integral on the right-hand side of (31) converges.

Once $\mu_t(y, z)$ is determined, $\mu_s(y, z)$ can be obtained directly from (3), where one of the two rays (either the a-type or the b-type) is employed. Finally, the absorption coefficient is obtained from the formula $\mu_a(y, z) = \mu_t(y, z) - \mu_s(y, z)$.

4. Numerical simulations

In this section, we illustrate the use of the inversion formulas with numerical examples. For the case of a constant scattering coefficient, we will use the Fourier-space formulas (22), (23) followed by the inverse Fourier transform (24) to reconstruct the total attenuation coefficient $\mu_t(y, z)$. For the case of a spatially varying scattering coefficient, the real-space formula (31) will be used to reconstruct $\mu_t(y, z)$ and the result will then be used to reconstruct μ_s and μ_a . In all cases, the reconstructions are carried out in a rectangular area $0 \leqslant z \leqslant L$, $0 \leqslant y \leqslant 3L$ and the detection angle is set to $\theta = \pi/4$, so that $\Delta_{\max} = L$.

In what follows, the optical coefficients are decomposed as

$$\mu_t(y, z) = \bar{\mu}_t + \delta\mu_t(y, z), \qquad \mu_s(y, z) = \bar{\mu}_s + \delta\mu_s(y, z), \qquad \mu_a(y, z) = \bar{\mu}_a + \delta\mu_a(y, z), \tag{32}$$

where quantities with an overbar are constant background values of the coefficients. In performing a reconstruction, it will be assumed that the support of the functions $\delta\mu_a(y, z)$ and $\delta\mu_s(y, z)$ is contained in the rectangular area where the image is reconstructed. This assumption is violated if Gaussian inhomogeneities are used, as will be done below. However, the resulting error is exponentially small.

4.1. Spatially uniform scattering

We consider first the case of a medium with $\delta\mu_s = 0$ and a spatially varying attenuation coefficient that is supported in a square domain:

$$\delta\mu_t(y, z) = \begin{cases} \bar{\mu}_t, & |y - y_0| \leqslant a/2 \quad \text{and} \quad |z - z_0| \leqslant a/2 \\ 0, & \text{otherwise} \end{cases}. \tag{33}$$

Thus, the attenuation coefficient inside the square is twice the background value of $\bar{\mu}_t$. The square is centered so that $y_0 = L$, $z_0 = L/2$ and its side length is $a = L/2$. The Fourier-space data function $\tilde{\psi}(k, \Delta)$ was obtained analytically from (22) by direct integration. Then the variables Δ and k were sampled and $\mu_t(y, z)$ was reconstructed using discrete samples of $\tilde{\psi}(k, \Delta)$. More specifically, the samples have been used to evaluate numerically equations (22) and (24). The variable Δ was sampled as $\Delta_n = hn$, where $n = 0, 1, \ldots, N$ and $h = \Delta_{\max}/N$. Note that for $\theta = \pi/4$, $\Delta_{\max} = L$. The Fourier variable k was sampled in the interval $[-\pi/h, \pi/h]$ according to $k_m = (\pi/h)(m/N - 1)$, where $m = 0, 1, \ldots, 2N$. The derivative in (23) was computed as the central difference

$$\left.\frac{\partial\tilde{\psi}(k, \Delta)}{\partial\Delta}\right|_{\Delta=\Delta_n} = \frac{\tilde{\psi}(k, \Delta_{n+1}) - \tilde{\psi}(k, \Delta_{n-1})}{2h}, \qquad n = 0, 1, \ldots, N. \tag{34}$$

In applying the above formula, the boundary condition $\tilde{\psi}(k, \Delta_{-1}) = \tilde{\psi}(k, \Delta_{N+1})$ has been used. Note that the substitution $\Delta \to (L - z)\tan\theta$ contained in the formula (23) did not require any resampling because, in the geometry used, $\tan\theta = 1$. More generally, however, resampling and interpolation is required to apply (23) to a uniformly sampled

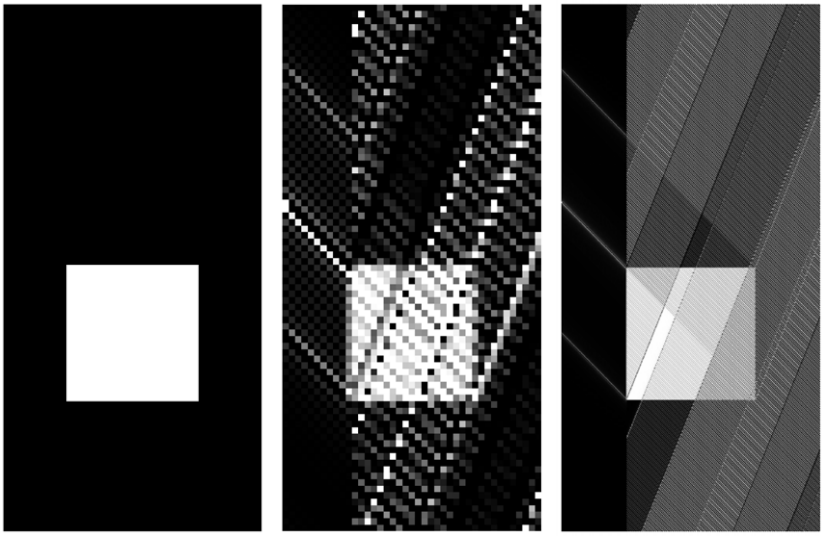

Figure 2. Reconstructed $\delta\mu_t(y, z)$ for the square inhomogeneity (33) using different numbers of samples N, as labeled.

function $\tilde{\psi}(k, \Delta)$. The integral over ℓ in (22) was evaluated numerically using the trapezoidal rule. Finally, the image was reconstructed on a rectangular grid with the same step size as was used to sample the variable Δ, that is, h. Reconstructions of the total attenuation coefficient $\mu_t(y, z)$, obtained as described above, are shown in figure 2 for two different values of the parameter N. It can be seen that the reconstruction contains artifacts. When the number of samples, N, is increased by a factor of 10, the support of the artifacts is reduced by the same factor, but the amplitude is unchanged. We have verified that the L^2 norm of the discrepancy $\xi(y, z) = \mu_t^{(\text{true})}(y, z) - \mu_t^{(\text{reconstructed})}(y, z)$ tends to zero when $N \to \infty$, yet the maximum amplitude of the relative error, $\max[\xi(y, z)/\mu_t^{(\text{true})}(y, z)]$, remains of the order of unity.

The relatively low image quality seen in figure 2 is due the jump discontinuity of $\delta\mu_t$. This statement is confirmed by considering a smooth inhomogeneity in which the attenuation coefficient is a Gaussian function of the form

$$\delta\mu_t(y, z) = \bar{\mu}_t \exp\left[-\frac{(y - y_0)^2 + (z - z_0)^2}{\sigma^2}\right]. \tag{35}$$

The corresponding Fourier-transformed data function, $\tilde{\psi}(k, \Delta)$, can be computed analytically. We have used the same sampling procedure as above and an image was reconstructed using equations (22)–(24). The results are shown in figures 3 and 4 where it can be seen that an accurate quantitative reconstruction is obtained. When a linear scale is used to represent the data, no artifacts are visible in the reconstructions and the reconstructed data coincide quantitatively with the model. However, when a logarithmic scale is used on the vertical axis, as is shown in panels (b), (d) of figure 4, the artifacts become clearly visible. The amplitude of the artifacts in the transverse cross section of the image (figure 4(b)) is, in fact, less than 2% of the plot maximum.

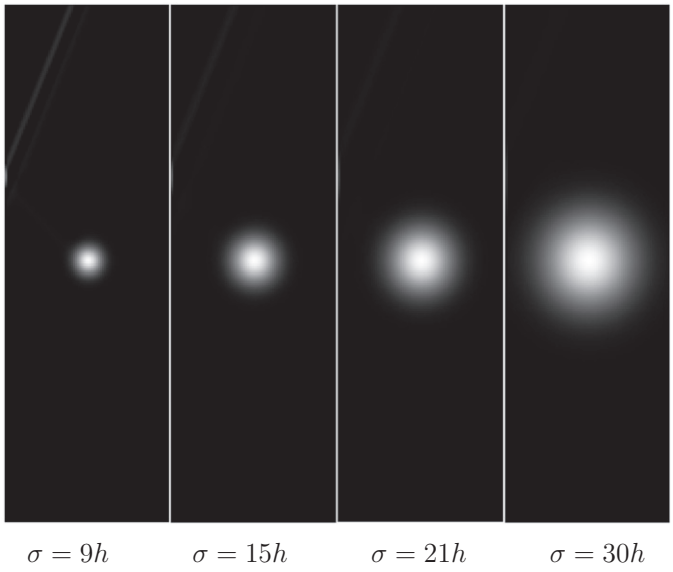

Figure 3. Reconstructed $\delta\mu_t(y, z)$ for the Gaussian inhomogeneity (35) using $N = 120$ and different values of σ, as labeled.

4.2. Spatially nonuniform scattering

We next consider the case when both the scattering and the absorption coefficients of the medium are spatially varying. We have modeled the inhomogeneities as Gaussian functions:

$$\delta\mu_{s,a}(y, z) = \bar{\mu}_{s,a} \exp\left[-\frac{(y - y_{s,a})^2 + (z - z_{s,a})^2}{\sigma^2}\right], \tag{36}$$

where (y_s, z_s) and (y_a, z_a) are the centers of the scattering and the absorbing inhomogeneities. Note that the amplitude of each coefficient in the center of an inhomogeneity is twice the background value. Both types of inhomogeneity are present in the medium simultaneously but not overlap. Thus, the scattering inhomogeneity was centered at the point $(y_s = 3.125L, z_s = 0.5L)$ and the absorbing inhomogeneity was centered at $(y_a = 0.875L, z_a = 0.5L)$. We have considered different values of the parameter σ. However, in each reconstruction, σ was the same for the absorbing and the scattering inhomogeneities.

In this subsection, we have used the real-space image inversion formula (31). The data function was obtained by analytical integration and the image reconstruction was performed by sampling the variables w and Δ in the data function $\psi_d(w, \Delta)$ on a rectangular grid with step size h, as described in more detail in the previous subsection. For the reconstructions of this subsection, $N = 120$ and $h = L/N$. The derivatives in (31) were computed by central differences and the integral by the trapezoidal rule.

We consider below two cases. The first case corresponds to $\bar{\mu}_s L = 2.4$ and $\bar{\mu}_a L = 0.24$. The challenge here is to reconstruct the absorbing inhomogeneities in the presence of much stronger scattering inhomogeneities. In the second case, $\bar{\mu}_s L = \bar{\mu}_a L = 2.4$, so that the strength of the absorbing and the scattering inhomogeneities is the same. Image reconstruction for the first case is illustrated in figures 5 and 6. Here we plot the total coefficients (including the background) rather than the fluctuating parts $\delta\mu_t$, etc., as was done in figures 2–4. It can be seen that quantitative agreement with the model is obtained for both the scattering and the

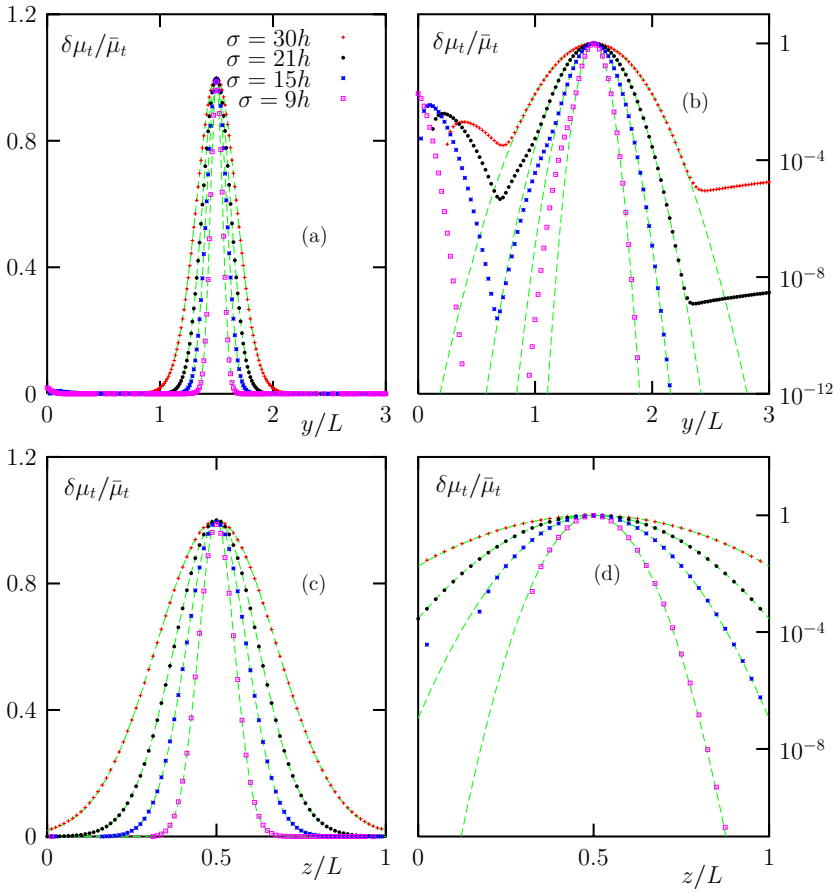

Figure 4. The data of figure 3 are shown here as cross sections along lines drawn through the center of the inhomogeneity in the directions parallel to the y-axis (a), (b) and to the z-axis (c), (d). The panels (a), (c) use a linear scale and the panels (b), (d) use a logarithmic scale for the vertical axis. Dots represent the reconstructed values and the model function is represented by the dashed lines. Every other reconstructed data point is shown in the semi-logarithmic plots. Some of the data points are not shown in the semi-logarithmic plots because their values are negative or too small to be displayed.

attenuation coefficients. We note that the accuracy of the reconstructed absorption coefficient is not as good as the scattering coefficient. This is because the relatively small quantity μ_a was obtained by finding the numerical difference between the two much larger quantities μ_t and μ_s. In the case when the magnitudes of the scattering and the absorbing inhomogeneities are the same, a quantitatively accurate reconstruction of all three coefficients is obtained, as is illustrated in figures 7 and 8.

5. Discussion

In conclusion, we have derived inversion formulas for the broken-ray Radon transform. The results we have obtained are analogous to the filtered backprojection formula for inversion of

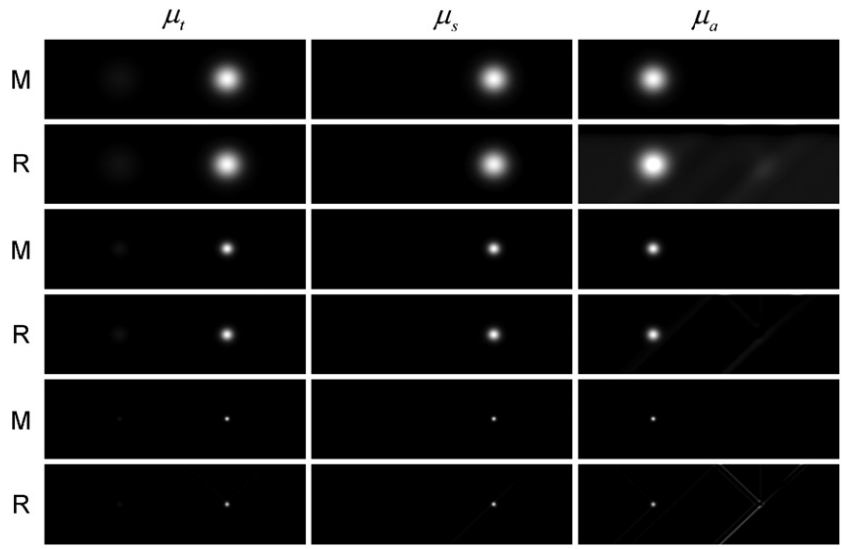

Figure 5. Simultaneous reconstruction of the absorption and scattering coefficients for the case $\bar{\mu}_s L = 2.4$, $\bar{\mu}_a L = 0.24L$. The three columns represent the attenuation, scattering and absorption coefficients, as labeled. The letter 'M' indicates 'model' and the letter 'R' indicates reconstruction. The first two rows correspond to $\sigma = 21h$, the next two rows correspond to $\sigma = 9h$ and the last two rows correspond to $\sigma = 3h$. Here $h = L/N$ and $N = 120$. Each plot is normalized to its own maximum.

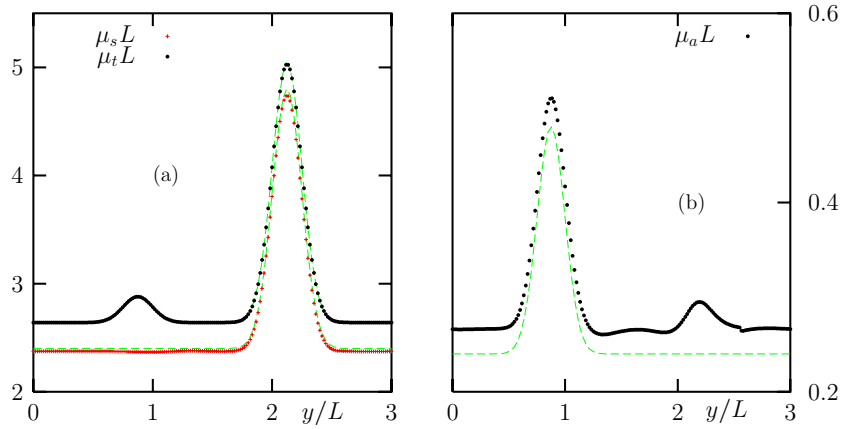

Figure 6. The data of figure 5 for the case $\sigma = 21h$ ($h = L/N$ and $N = 120$) are shown here as cross sections along the straight line $z = z_a = z_s$, which intersects the centers of the absorbing and the scattering inhomogeneities. The total attenuation and scattering coefficients are shown in panel (a) and the absorption is shown in panel (b). Centered symbols correspond to the reconstructed values and the dashed lines correspond to the model.

the two-dimensional Radon transform. Numerical simulations were conducted to illustrate the method in model systems.

We conclude with several remarks. (i) Imaging with ballistic photons allows only for the recovery of the attenuation coefficient $\mu_t = \mu_a + \mu_s$. In contrast, inversion of the broken-

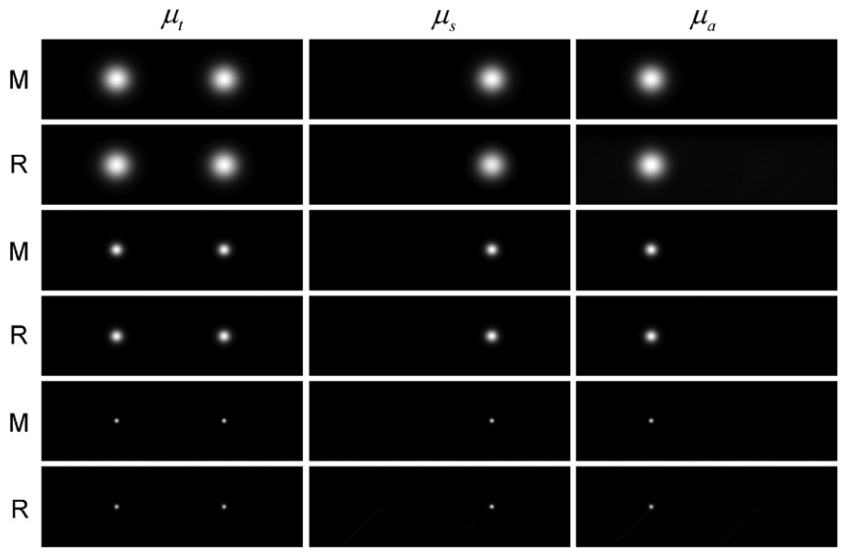

Figure 7. As in figure 5 but $\bar{\mu}_s L = \bar{\mu}_a L = 2.4$.

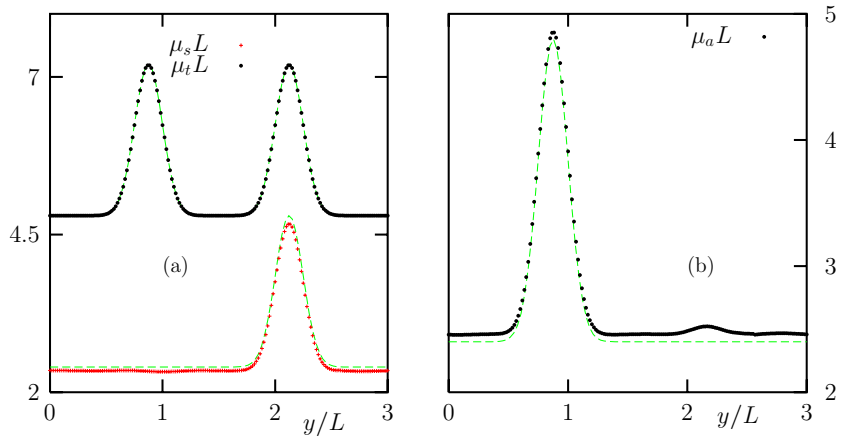

Figure 8. As in figure 6 but $\bar{\mu}_s L = \bar{\mu}_a L = 2.4$.

ray transform in SSOT allows for separate reconstructions of the absorption and scattering coefficients. (ii) Inversion of the broken-ray transform is mildly ill-posed [6]. The ill-posedness strongly affects image reconstruction when the inhomogeneity has singularities. We conjecture that the ill-posedness can be regularized by making use of additional measurements. (iii) It is well known that the filtered backprojection inversion formula for the Radon transform produces blurry images for the case of limited-angle data. In particular, one can stably reconstruct only singularities that can be tangentially touched by the integration paths, while all the other singularities are blurred. We note that an analogous effect is *not* observed in figure 2, where the reconstructions are of high quality even for jump discontinuities that are not parallel to the paths of the broken rays. It would thus be of interest to study the propagation

of singularities for the broken-ray Radon transform. Related theoretical questions concern mapping properties and range conditions of the transform. We plan to investigate these topics in future work. (iv) Since the Radon transform is a special case of the broken-ray Radon transform, it may be of interest to investigate imaging modalities that make use of ballistic- and single-scattered photons simultaneously. This will be the subject of future work. (v) In gamma-ray emission tomography the physical mechanism of image formation is related to single Compton scattering of gamma rays. It has been shown that the problem of reconstructing the density of the source of gamma rays is related to inverting the so-called V transform [3]. The V transform is a special case of the broken-ray transform in which the position of the source and the orientation of the detector are varied. A generalized filtered backprojection inversion formula for the V transform has recently been reported [8].

Acknowledgments

This work was supported by the NSF under the grants DMS-0554100 and EEC-0615857, and by the NIH under the grant R01EB004832. The authors are grateful to Guillaume Bal, Alexander Katsevich, Peter Kuchment, Shari Moskow, Todd Quinto and Plamen Stefanov for stimulating discussions. We also thank the referees for valuable suggestions.

References

[1] Arridge S R and Schotland J C 2009 Optical tomography: forward and inverse problems *Inverse Problems* **25** 123010
[2] Bal G 2009 Inverse transport theory and applications *Inverse Problems* **25** 053001
[3] Basko R, Zeng G L and Gullberg G T 1997 Analytical reconstruction formula for one-dimensional Compton camera *IEEE Trans. Nucl. Sci.* **44** 1342–6
[4] Choulli M and Stefanov P 1996 Inverse scattering and inverse boundary value problems for the linear Boltzmann equation *Commun. Partial Diff. Eqns.* **21** 763–85
[5] Choulli M and Stefanov P 1999 An inverse boundary value problem for the stationary transport equation *Osaka J. Math.* **36** 87–104
[6] Florescu L, Schotland J C and Markel V A 2009 Single-scattering optical tomography *Phys. Rev.* E **79** 036607
[7] Florescu L, Markel V A and Schotland J C 2010 Single-scattering optical tomography: simultaneous reconstruction of scattering and absorption *Phys. Rev.* E **81** 016602
[8] Morvidone M, Nguyen M K, Truong T T and Zaidi H 2010 On the V-line radon transform and its imaging applications *Int. J. Biomed. Imaging* 208179
[9] Stefanov P and Uhlmann G 2003 Optical tomography in two dimensions *Methods Appl. Anal.* **10** 1–9
[10] Kurylev Y, Lassas M and Uhlmann G 2010 Rigidity of broken geodesic flow and inverse problems *Am. J. Math.* **132** 529–62